

Annual Review of Materials Research
Using Severe Plastic
Deformation to Produce
Nanostructured Materials
with Superior Properties

Ruslan Z. Valiev,¹ Boris Straumal,²
and Terence G. Langdon³

¹Institute of Physics of Advanced Materials, Ufa State Aviation Technical University, Ufa, Russia; email: ruslan.valiev@ugatu.su

²Osipyan Institute of Solid State Physics, Russian Academy of Sciences, Chernogolovka, Russia

³Materials Research Group, Department of Mechanical Engineering, University of Southampton, Southampton, United Kingdom

Annu. Rev. Mater. Res. 2022. 52:357–82

First published as a Review in Advance on
April 28, 2022

The *Annual Review of Materials Research* is online at
matsci.annualreviews.org

<https://doi.org/10.1146/annurev-matsci-081720-123248>

Copyright © 2022 by Annual Reviews.
All rights reserved

Keywords

bulk nanostructured materials, severe plastic deformation, ultrafine-grained biomaterials, functional properties, mechanical properties, nanostructural design

Abstract

The past decade was marked by significant advances in the development of severe plastic deformation (SPD) techniques to achieve new and superior properties in various materials. This review examines the achievements in these areas of study and explores promising trends in further research and development. SPD processing provides strong grain refinement at the nanoscale and produces very high dislocation and point defect densities as well as unusual phase transformations associated with particle dissolution, precipitation, or amorphization. Such SPD-induced nanostructural features strongly influence deformation and transport mechanisms and can substantially enhance the performance of advanced materials. Exploiting this knowledge, we discuss the concept of nanostructural design of metals and alloys for multifunctional properties such as high strength and electrical conductivity, superplasticity, increased radiation, and corrosion tolerance. Special emphasis is placed on advanced metallic biomaterials that promote innovative applications in medicine.

**ANNUAL
REVIEWS CONNECT**

www.annualreviews.org

- Download figures
- Navigate cited references
- Keyword search
- Explore related articles
- Share via email or social media

1. INTRODUCTION

Processing by severe plastic deformation (SPD) is one of the most efficient means for fabricating bulk ultrafine-grained (UFG) metals and alloys. Pioneering research in this area has been conducted for over 25 years (1, 2). **Figure 1** illustrates the recent growth in research activity on SPD (3). Most trends in SPD research are thoroughly described in several recently published review articles and books covering different aspects of nanostructured materials from SPD processing, such as simulation and development of SPD techniques (1, 4–7); grain refinement and its mechanisms in various materials, such as pure metals, model and commercial alloys (2, 3, 6, 8–10), intermetallic compounds, and some ceramics and polymers (10–12); and fundamentals of superior properties and the innovative potential of nanostructured materials processed by SPD (1, 2, 12–17).

Recent studies demonstrated that SPD processing allows the introduction of effective grain refinement as well as nontypical phase transformations (3, 14). These processes result in the formation of peculiar, nonequilibrium structural features at the nanoscale, such as high dislocation densities located mainly at grain boundaries (GBs) (1, 18), nanotwins (13), solid solution decomposition in alloys leading to the formation of nanoprecipitates (14, 16), and the redistribution of alloying elements segregating at GB areas (8, 18). Especially remarkable is the unusual combination of SPD-induced diffusive and displacive (martensitic) phase transformations (19, 20).

These SPD-induced nanostructural features influence deformation mechanisms in SPD materials and lead to substantial enhancement of their performance to a degree that cannot be attained by conventional processing. Exploiting this knowledge opens a new way of formulating the concept of nanostructural design by SPD processing and for evolving superior multifunctional properties in UFG materials.

The past decade has been marked by significant progress in developing and optimizing SPD processing techniques to achieve superior properties. These developments are associated either with modifications of the conventional SPD techniques to promote their commercialization (such as an improvement in the efficiency of processing techniques and a reduction of material wastage) (4, 7, 21, 22) or with the optimization of SPD regimes and the development of complex SPD

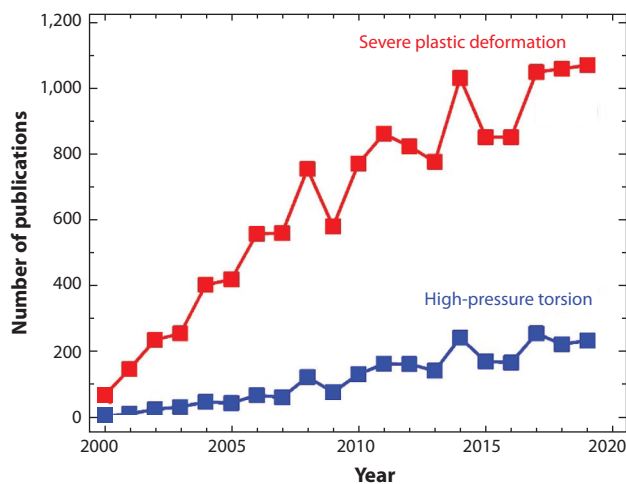


Figure 1

Numbers of papers published on research in severe plastic deformation and high-pressure torsion. Data were collected from Scopus on April 23, 2020, and the papers were counted from those published in peer-reviewed journals, including proceeding papers screened by reviewing processes. Figure adapted from Reference 3.

processing routes when two or more SPD processing techniques are combined (23, 24). Complex SPD processing routes applied to metallic materials provide further microstructural refinement and therefore higher reductions in grain size, resulting in drastic improvements in performance. A combination of several processing techniques provides an extra tool for texture design in UFG metallic materials to further control the anisotropy of microstructure and the resulting properties.

The present article provides a critical review of the latest achievements in advanced SPD processing, focusing on developments that have not received appropriate attention in earlier reviews. Historical developments and a short overview of the most popular (classical) SPD processing techniques are presented briefly in the beginning of Section 2. Modified SPD processing techniques and regimes are described in Section 2.1, followed by a presentation of complex SPD processing routes applied for nanostructuring of various metals and alloys in Section 2.2. Microstructural features of UFG materials produced by advanced SPD processing, as well as the main principles of nanostructural design via SPD to achieve superior mechanical and functional properties, are presented and discussed in Sections 3 and 4. The existing and potential applications of UFG metals via advanced SPD processing are outlined and discussed in Section 4.

2. RECENT TRENDS IN THE DEVELOPMENT OF SPD TECHNIQUES

The processing of nanomaterials by SPD techniques has become a popular topic in research laboratories around the world. From a historical point of view, SPD processing is relatively young, but its basic idea goes back to the work of ancient artisans who used a repetitive forging and folding technique (2). This process was first developed for steel manufacturing in China for use in swords about 2,000 years ago. The processing approach was also employed for manufacturing Wootz steel in Japan and later in India. This processing concept then spread further to the Middle East, where the famous Damascus steel was developed. Impressively, all these processing techniques were developed without metallurgical knowledge and without any fundamental understanding of the basis for the processing procedures.

Edalati & Horita (25) recently carried out a detailed analysis of research activities related to SPD from 1935 to 1988. In 1935, Prof. P.W. Bridgman of Harvard University (26) introduced a die set for compression and torsion straining and conducted the first studies of the effects of high hydrostatic pressure combined with high shear stress on phase transformations in minerals and metals. The principles of Bridgman's fundamental work were further extended using die sets combining shear (torsion) and compression straining to introduce high shear strain without changing the sample shape. Such experimental die sets were developed in the 1980s by Polish and British scientists and by Russian scientists from Yekaterinburg (formerly Sverdlovsk, USSR) (see 25). Very large strains, with true strains exceeding 6–8, were achieved using these facilities, leading to significant microstructural refinement in several metals.

The year 1988 included another milestone. A pioneering study on SPD processing was performed in Ufa (27), resulting in the production of metals and alloys with submicrometer grain sizes and high-angle GBs that showed outstanding superplastic properties. This was further studied in the works of Valiev and colleagues (28) using a combination of torsion and compression, later termed high-pressure torsion (HPT), with the Bridgman type of die set. A short time later, this research was extended to equal-channel angular pressing (ECAP) (29). The results of these early studies are summarized in Reference 1.

HPT and ECAP have become the most popular SPD processing techniques, although these processes are being continuously modified, as described below. Furthermore, several other SPD processing techniques are now also available, including accumulative roll bonding (ARB), twist extrusion, and multiaxis forging. Several recent reviews and books (7, 24, 30, 31) focus on the

different SPD techniques and provide detailed information about their main principles and recent developments.

However, these SPD techniques have been used primarily for laboratory-scale research. The requirement for economically feasible production of UFG metals and alloys raises several new problems in the development of SPD processing. The key challenges are to reduce material waste, obtain a uniform UFG structure and enhanced properties in bulk billets and products, and increase productivity. Strategies for solving these problems are examined in the following section.

2.1. Continuous SPD Processing Techniques

To increase the efficiency of SPD techniques, continuity is the key to obtaining long-sized products and ensuring high processing efficiency. Over the past decade, this challenge has been successfully completed for both SPD techniques: ECAP and HPT.

2.1.1. Continuous equal-channel angular pressing. The conventional ECAP process is very labor intensive, since it requires significant manual effort related to inserting and removing the relatively short billets (typically having lengths of approximately 100–200 mm) from conventional dies. Therefore, the conventional ECAP technique was modified into continuous forms that can be used for efficient production of material in relatively large volumes with lower waste (4). Early research focused on the development of continuous ECAP procedures combined with a rolling mill or drawing, with the aim of processing long metal strips and rods (see 7). However, further modification of these techniques was required for processing materials with UFG structures.

Rosochowski & Olejnik (32) proposed another modification of the ECAP technique for processing of long samples. This incremental ECAP (I-ECAP) is a cyclical process in which the billet is delivered into the deformation zone, where a small volume of material is deformed by simple shear in each cycle by a reciprocating punch. This technique was further modified into a double-billet I-ECAP process (33).

Continuous pressing was first proposed by Segal et al. (34) as a continuous simple shear process of long rods based on the famous Conform process. The ECAP with a Conform (ECAP-C) procedure was first developed and used for grain refinement in commercially pure aluminum down to 650 nm (35). Today, this technique is termed the ECAP-C process (**Figure 2**), and it has been used in laboratories around the world (4, 22, 23, 36–38).

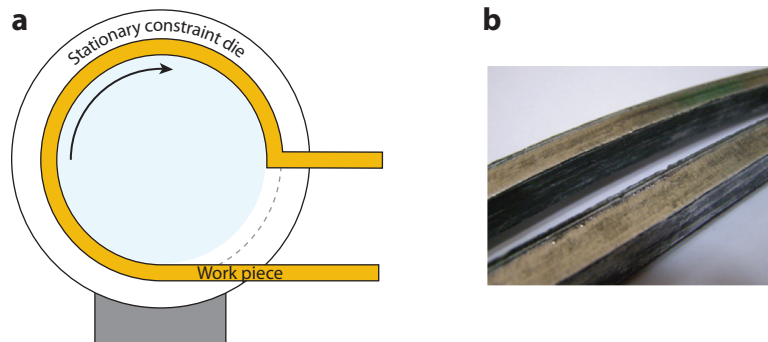


Figure 2

(a) A schematic illustration of an equal-channel angular pressing–Conform (ECAP-C) device and (b) Al billets after six ECAP-C passes. Panel a adapted with permission from Reference 35. Panel b adapted with permission from Reference 39.

Similar to what occurs with the conventional ECAP technique, ECAP-C samples may be subjected to various processing routes and regimes, as described in detail in Reference 4. Computer modeling of ECAP-C is widely applied for selection of load-bearing elements and materials (23, 39). ECAP-C can be applied not only to easily deformable materials, such as commercially pure Al, but also to various alloys, commercially pure Ti, and steels (22, 23, 38, 39).

A combination of ECAP-C with other deformation processing techniques (such as drawing and rolling) can achieve superior mechanical and functional properties in metallic materials, and this topic is considered in detail in Section 5. The ECAP-C process can be used to process metallic rods with UFG microstructure, yielding much higher mechanical and functional properties than conventional coarse-grained counterparts.

2.1.2. Continuous and modified high-pressure torsion techniques. The HPT process is another very popular SPD technique, although it has three main limitations (5, 21):

1. Small disks produced by HPT are not suitable for most industrial applications;
2. The high degree of applied pressure that must be maintained through straining introduces a limit on the installation construction; and
3. An inhomogeneous degree of strain is induced across the diameters of the disks, resulting in microstructural and property gradients.

A modified HPT technique for the processing of rings introduced by Harai et al. (40) helps to overcome some of these limitations. The replacement of a disk by a ring permits not only the avoidance of the less-processed central part of the disk but also a further scaling-up of the HPT technique to 100 mm in diameter (41). The sample shape can be improved by high-pressure sliding (HPS), which is another attempt that was developed for fabrication of sheet metallic materials that are 100 mm long, 5 mm wide, and 0.8 mm thick (42).

The HPS technique is shown in **Figure 3**. Rectangular sheets can be processed using HPS, and the process may be scaled up once an equal strain is introduced throughout the sample under the same load.

Continuous HPT (CHPT), developed with the aim of microstructural refinement and subsequent enhancement of properties, was the next step in the improvement of HPT (43). CHPT was successfully applied for manufacturing of 2-mm-diameter UFG wires from pure Al and Cu.

A new incremental HPT technique was also proposed recently (44). This technique offers new possibilities for processing UFG metallic materials and appears attractive from the viewpoint of

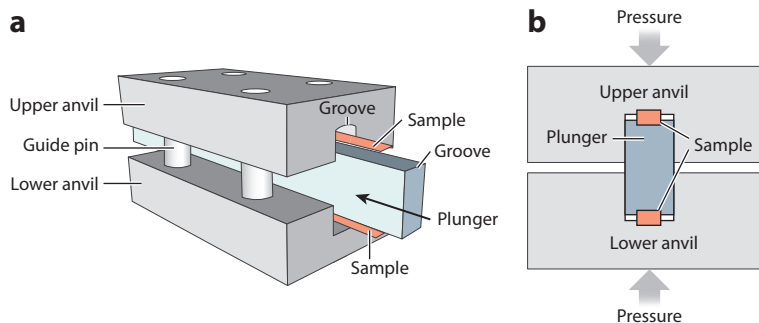


Figure 3

Illustration of high-pressure sliding. (a) Assembly of two anvils with guiding pins, one plunger, and two thin sheet samples. (b) Cross-sectional view of assembly. Figure adapted with permission from Reference 42.

industrial applications, as it allows HPT processing of cylinders instead of disks. The method is worthy of further development, as are investigations of its effect on the microstructure and properties of various materials.

2.2. Complex SPD Processing Routes

Processing by combinations of several deformation processing techniques, including at least one SPD technique, is often referred to as complex SPD processing routes. For example, two-step SPD processing, such as ECAP followed by HPT, was reported to induce additional refinement in the grain size and a consequent increase in mechanical strength and ductility (45). In the section below, the main features of complex SPD processing are considered, as is its influence on the microstructure and properties of numerous metals and alloys.

2.2.1. Combinations of two and more SPD techniques. Different combinations of SPD techniques used for processing of metallic materials can be found in the literature [e.g., ECAP and HPT (5, 46–48), ECAP and hydrostatic extrusion (49), and ECAP and ARB (50), all applied to various metallic materials]. Typically, a combination of SPD processing techniques leads to microstructures that are quite different from those obtained if the material is processed by an individual SPD technique. This includes extreme grain refinement; variations in morphology, size, and fractions of second-phase precipitates; dislocation structure and density; crystallographic texture and microtexture; and GB misorientations.

Grain refinement and further nanostructural modification in metallic materials processed using complex SPD routes generally result in improved mechanical properties (47, 49). However, the microstructure evolution during processing using combined SPD techniques also depends on the processing regimes (i.e., homologous temperature and strain) and chemical composition of the material (i.e., its thermal stability). This was clearly seen for pure Ti processed by ECAP and then subjected to HPT at 450°C and at room temperature (45). The latter processing resulted in a much finer grain size and higher mechanical strength.

A combination of SPD techniques was also used for grain refinement in a commercial ZK60 magnesium alloy to improve its functional properties. In a recent report (50), the hydrogen storage properties of this alloy were investigated after ECAP processing for 6 passes and ARB processing for 25 passes. The average grain size was approximately 0.8 μm after ECAP and was further reduced to around 0.3 μm after ARB processing. The latter also resulted in the formation of basal texture with (002) planes parallel to the rolling surface. The hydrogen absorption and desorption kinetics were also measured. Processing only by ECAP resulted in a very low hydrogen storage capacity of 0.5 weight percent (wt. %). Additional processing by ARB refined the microstructure and improved the hydrogen absorption. The sample from the ECAP material absorbed 4.77 wt. % of hydrogen in 24 h, whereas the capacity of the sample processed by ECAP and ARB was 6.4 wt. %. The enhanced kinetics of hydrogen absorption and desorption in the alloy after additional ARB processing were related to the finer grain size, since hydrogen diffusion is generally faster along GBs and the GBs and GB triple junctions can act as nucleation sites for the hydride phase.

2.2.2. SPD processing with traditional metal-forming techniques. After simple SPD processing, samples can also be subjected to deformation by a conventional metal-forming technique (such as rolling, drawing, or extrusion) or by a combination of techniques. This may be conducted to change the shape of the sample, to further modify the microstructure and properties, or both. For example, the application of rolling allows the fabrication of UFG sheets from SPD-processed billets or rods. Several combinations of SPD techniques with deformation processing methods are reported in the literature. For example, ECAP was combined with rolling at various temperatures

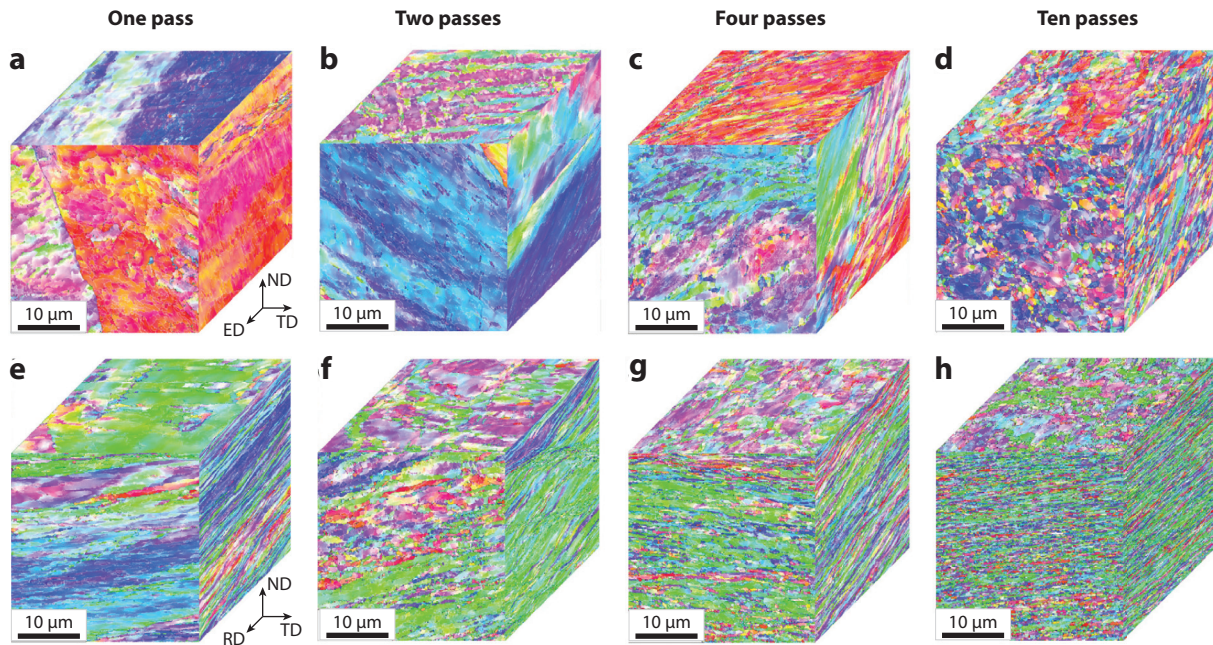


Figure 4

Electron back-scattering diffraction (EBSD) orientation maps of Cu after equal-channel angular pressing (ECAP) (*a–d*) and ECAP with subsequent rolling (*e–h*) for one pass (*a,e*), two passes (*b,f*), four passes (*c,g*), or ten passes (*d,h*). Low-angle boundaries ($2^\circ \leq \theta < 15^\circ$) and high-angle boundaries ($\theta \geq 15^\circ$) are shown on EBSD maps using white and black lines, respectively. Abbreviations: ED, extrusion direction; ND, normal direction; RD, rolling direction; TD, transverse direction. Figure adapted with permission from Reference 56.

(51, 52), with extrusion (53), with swaging and drawing (54), and with forging and drawing (55), and ECAP-C was combined with drawing (23). Analysis of these results shows that the final microstructure, properties, and shape of the processed material are determined by both microstructure and texture of the SPD-processed material before the metal-forming operation (or operations) and the parameters of the metal-forming operation (temperature, strain, strain rate, and strain path).

The microstructure and mechanical properties of commercially pure Cu after 1–10 ECAP passes using route B_C were compared with those of samples further cold rolled to a total reduction ratio of 90% (56). Cold rolling caused a transformation of the relatively equiaxed UFG structure developed in Cu during ECAP processing into a lamellar structure with even finer boundary spacing (**Figure 4**). For example, a boundary spacing approaching 180 nm after 10 ECAP passes decreased to approximately 110 nm after rolling (**Figure 4g,h**). A negligible grain refinement in terms of the formation of new boundaries takes place during rolling of ECAP-processed Cu. Cold rolling after ECAP with a corresponding number of passes also led to a significant increase (about 20%) in the average fraction of high-angle GBs.

The metal-forming parameters of cold rolling after ECAP also significantly affect the microstructure, texture, and mechanical properties of SPD-processed material. This was clearly demonstrated for commercially pure Ti (57, 58) subjected to a two-step process consisting of ECAP (at 300°C) and cold rolling with a reduction ratio of 70–76% (at room temperature or at liquid nitrogen temperature). Such processing served to activate two strengthening mechanisms in the pure metal: GB strengthening due to the grain size reduction from the ECAP processing

and dislocation strengthening from deformation by rolling. A reduction of rolling temperature from 20°C to cryogenic temperature improved the yield strength of the two-step processed pure Ti (ECAP for six passes followed by rolling) from about 785 MPa to about 915 MPa due to an increased dislocation density in the cryorolled material (57).

Clear advantages of combining ECAP with further thermomechanical treatment have been demonstrated in the development of Ti-based materials for biomedical applications (23, 59), including shaping semiproducts in the form of sheets or rods and enhancement of properties introduced by ECAP in UFG materials (see also Section 4.3 on nanostructured metallic biomaterials).

The development of complex SPD processing routes for fabrication of UFG materials is usually based on numerous experimental trials and is a very time-consuming and expensive process requiring a significant amount of material and a precise analysis of microstructure, thermal stability, and mechanical properties. Thermomechanical simulation of the metal-forming processes helps to minimize the amount of expensive SPD-processed material needed for such experimental work, increases the efficiency of the work, and thus reduces the cost (23, 60). The results may be used directly in the laboratory as well as in full-scale production.

A physical simulation of hot rolling of ECAP-processed UFG pure Ti was carried out (60) using $20 \times 15 \times 5 \text{ mm}^3$ samples to predict microstructure and texture evolution, as well as the microhardness, during hot rolling. It was demonstrated that hot rolling leads to a breakup of the ECAP-type crystallographic texture, a further refinement of grain size, and an improvement in microhardness with increasing total reduction ratio.

Recently, a modified method called HPT extrusion (HPTE) was proposed (61). This technique combines HPT and cyclic extrusion. HPTE used for processing bulk nanostructured materials in quantities suitable for industrial applications has several advantages: simple shear conditions, high hydrostatic pressure in a rod-shaped specimen, and the accumulation of a large strain in a single pass. Furthermore, hybrid materials with helical architecture, gradient materials, and such can be produced in a rather simple way using this newly developed process.

3. NANOSTRUCTURAL ARCHITECTURE OF SPD-PROCESSED MATERIALS

Studies performed during the past decade, using techniques including 3D atom probe tomography (APT), transmission electron microscopy (TEM), high-resolution TEM (HRTEM), and X-ray diffraction, revealed that SPD processing not only can form ultrafine grains but also may be used to engineer GB structures and generate nanoparticles, segregation, or nanoclusters and other structural elements at the nanoscale. The nature of these phenomena is related to the fact that, together with grain refinement, processing by SPD may also lead to unusual phase transformations as a dissolution of second phases, precipitation, amorphization, allotropic phase transformations, and other nanostructural features (see, for example, 12, 14, 16, 18). Also, the unusual combinations of SPD-induced diffusive and displacive (martensitic) phase transformations (i.e., transitions with or without mass transfer) can take place during SPD (19, 20, 62). By contrast, the type and morphology of such nanostructural elements, as well as their number density, control deformation and transport mechanisms responsible for improvements in the mechanical, chemical, and physical properties of bulk nanostructured materials through SPD techniques and the optimization of processing regimes. Nanostructuring via SPD processing is considered in this section.

3.1. Grain Boundaries in Nanostructured Materials

The density of GBs and interphase boundaries in UFG materials with submicron (100–1,000 nm) or nanocrystalline (<100 nm) sizes is very high and can significantly impact properties. UFG materials can thus be considered as interface-controlled materials (63, 64).

Gleiter (64) suggested that the atomic structure of GBs in UFG materials may be characterized by several special features, in contrast to GBs in conventional polycrystalline materials. This is especially important for materials in which UFG microstructures are produced by SPD techniques (1, 12, 18).

Although the physical mechanisms of microstructure evolution during SPD processing call for further investigation, numerous studies demonstrate that the formation of a UFG structure is determined by the evolution of cells or dislocation substructures formed in the early deformation stages into ultrafine grains with high-angle boundaries during subsequent deformation. At the same time, and depending on the regimes of SPD processing, different types of GBs can be formed in the UFG materials, such as high and low angle, special and random, and equilibrium and so-called nonequilibrium GBs with strain-distorted structures containing extrinsic dislocations, as well as boundaries with GB segregation of alloying elements (16, 18).

As discussed in Section 2, the fabrication of UFG metals and alloys with predominantly high-angle GBs by SPD techniques was first revealed by Valiev et al. (1) and colleagues (2, 25). In the past decade, active development and application of electron back-scattering diffraction (EBSD) have provided quantitative data on the low- to high-angle GB ratio and the presence of special and random boundaries in various metals and alloys subjected to SPD. For example, EBSD analysis has been used to plot misorientation histograms (65). A Mackenzie plot has been added to each histogram for an ECAP-processed Al 6016 alloy. The boundary misorientation angle histogram in **Figure 5** shows that after the first ECAP pass, the microstructure is characterized by approximately 93% of the boundaries with misorientation angles $<15^\circ$ (i.e., low-angle boundaries).

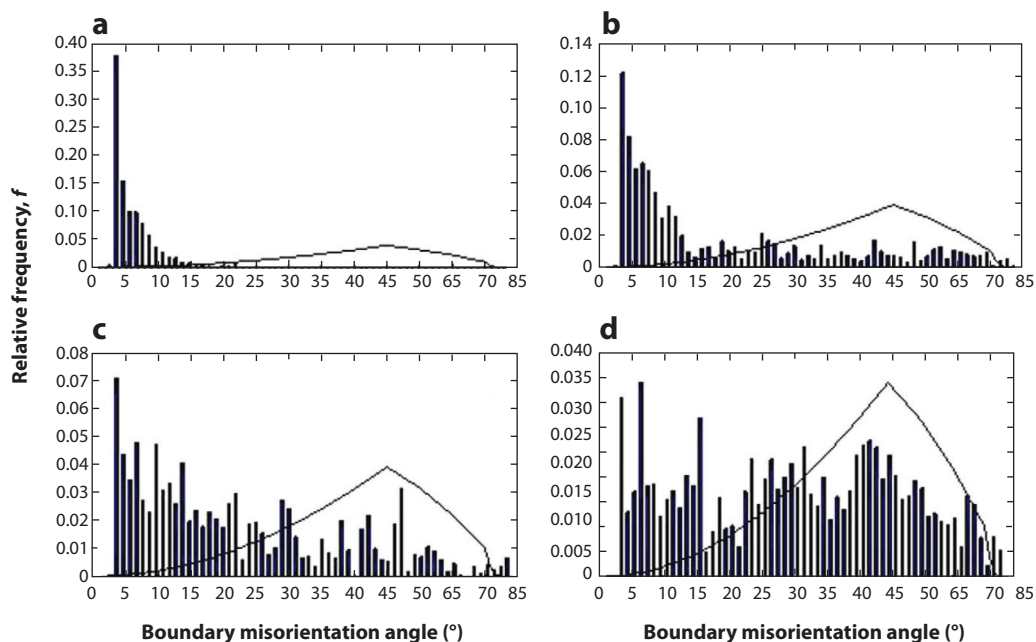


Figure 5

Relative frequency of dislocation cell or subgrain boundaries as a function of misorientation angle for Al 6016 samples processed by equal-channel angular pressing. (a) One pass, (b) two passes, (c) four passes, and (d) eight passes with a Mackenzie plot (i.e., the distribution of misorientation angles for a randomly textured polycrystal) superimposed on each histogram. Figure adapted with permission from Reference 71.

After the second pass (**Figure 5b**), the average dislocation cell size is reduced considerably, but the inhomogeneous structure remains characteristic for most cells orientated parallel with the Y (or transverse) direction. Simultaneously, the boundary misorientation distribution shifts upward, with about 67% of boundaries comprising misorientation angles $<15^\circ$. After four ECAP passes, some equiaxed dislocation cells or subgrains appear together with some shape irregularities and alignment of the microstructure off-axis to the Y (or transverse) direction. The distribution histogram with approximately 34% of boundaries having a misorientation of $<15^\circ$ reflects a more gradual upward shift in the corresponding misorientation angle (**Figure 5c**). Further processing to eight passes resulted in an evident reduction of the dislocation cell or subgrain size and upward shifts in the misorientation distributions (**Figure 5d**). A near-random distribution after 12 ECAP passes was observed (65).

The results of this work, as well as another recent study by EBSD analysis (66), provide convincing support for earlier conclusions that the formation of a UFG structure with mostly high-angle boundaries takes place during ECAP when the number of passes is greater than four to six (true strain is greater than four to six). Such very large strains cannot be achieved using conventional processing techniques, such as rolling, extrusion, or drawing, and therefore their application provides no opportunity for the formation of a real UFG microstructure with mostly high-angle GBs. Moreover, SPD techniques involve simple shear, which makes it possible to form the ultra-fine grains as equiaxial or at least close to it in shape.

A variety of characterization methods—including high-resolution TEM (HRTEM), X-ray diffraction, Mössbauer spectroscopy, dilatometry, and differential calorimetry (see, for example, 1, 10, 16)—were used in different studies to investigate features of GBs in UFG materials produced by SPD techniques. These studies clearly demonstrated that optimization of the SPD processing regimes results in the formation of mostly high-angle GBs with specific nonequilibrium structures. The application of GB diffusion measurements (67–69) and HRTEM analyses (18, 70, 71) helped identify and characterize the effect of the severe deformation processing on transformations of the GB structures. For example, it was revealed that HPT may result in the formation of a very high density of dislocations, facets, and steps at GBs in the Al-3% Mg UFG alloy (72). Numerous reports confirm the appearance of such nonequilibrium GBs in different materials processed by SPD (1, 18, 69, 73).

The term nonequilibrium GBs has been accepted and is used by the entire SPD materials science community. It is also used here to describe GBs that are defined formally as boundaries with strain-distorted structures and high densities of extrinsic dislocations (1, 18).

Thus, recent studies of the GB structure in SPD-processed UFG materials suggest that specific nonequilibrium GBs with strain-distorted structures associated with a correspondingly large residual microstrain are a typical feature in these nanomaterials.

3.2. Nanotwins in Metallic Nanomaterials

Decreasing grain size usually impedes twinning in coarse-grained, face-centered-cubic metals. In nanocrystalline metals, twinning becomes easier with decreasing grain size up to a certain grain size, reaching a maximum twinning probability, and then twinning becomes more difficult when the grain size decreases even further (74). The difference between twinning mechanisms in nanocrystalline and coarse-grained materials has been revealed by molecular dynamics simulations and experimental observations.

The formation of nanotwins can be promoted if certain properties intrinsic to the material and external deformation conditions are satisfied, including a relatively low stacking fault energy, a low deformation temperature, and a high strain rate (74). A range of grain sizes is apparently optimal for deformation twinning for different materials and testing conditions. In particular,

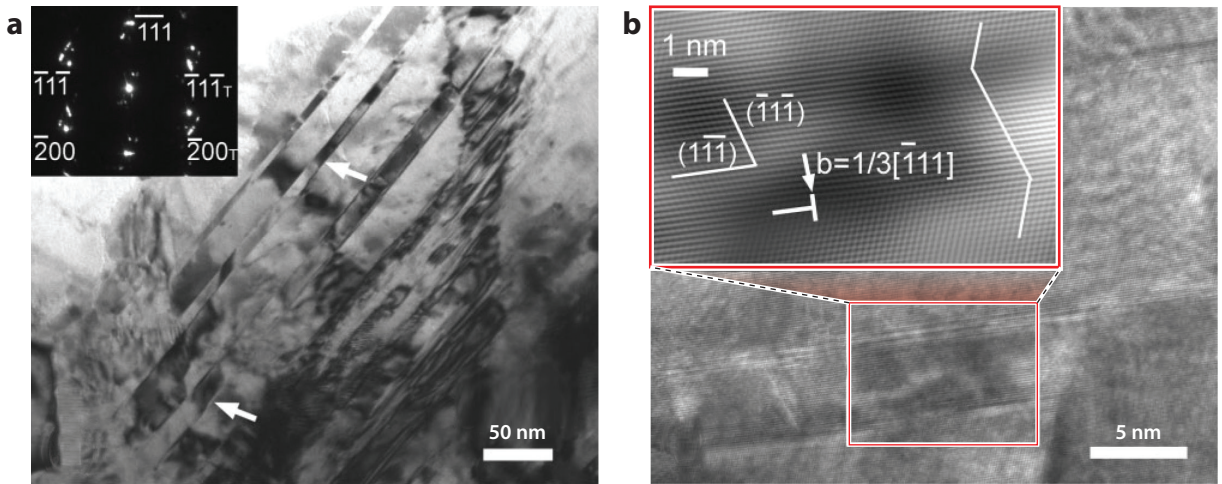


Figure 6

Transmission electron microscopy images of a typical grain with a high density of deformation twins in ultrafine-grained Cu processed by equal-channel angular pressing with subsequent cold rolling. (a) The white arrows indicate the positions of the twins, and the diffraction pattern from this region is provided. (b) Inset is a high-resolution transmission electron microscopy image of this region with its atomic-crystalline structure indicated. Figure adapted with permission from Reference 75.

lower temperatures, additional cold rolling, extrusion, and drawing can all promote the formation of nanotwins. **Figure 6** shows an HRTEM image of UFG Cu after ECAP and cold rolling at liquid nitrogen temperature. In it, 10–20-nm twins can be clearly observed (75). Enhanced strength and ductility can also be obtained in nanocrystalline materials due to deformation twinning (75, 76).

Twin GBs (even in nanotwins) typically contain high-energy facets in addition to the main low-energy $\Sigma 3$ $\{111\}1//\{111\}2$ facet (Σ is the reverse bulk density of the coincidence sites). The observation of such high-energy facets in materials after SPD is evidence of nonequilibrium GBs processed by SPD (77).

3.3. Segregation in SPD-Processed Nanostructured Alloys

Several investigations of thermal stability as a function of the impurity level in metals have supplied indirect evidence of GB segregation in UFG materials. However, GB segregation has recently been observed in UFG materials processed by SPD directly (18, 73, 78–80). APT is the main technique used for atomic-scale characterization in most of these reports. Crystallographic information provided by this technique is very limited, and the GB misorientation usually cannot be determined. Moreover, there is almost no possibility of statistical analysis because of the very small GB areas that are analyzed. Nevertheless, the demonstration of GB segregation in various SPD-processed metallic materials confirms that this is not a marginal feature.

SPD processing resulted in the formation in a UFG AA6061 alloy with a microstructure characterized by Mg, Cu, and Si segregation along planar defects attributed to GB (78). The thickness of the layer enriched by solute elements was about 2 nm. The local enrichment was <2 atomic percent (at. %). Segregation at GB was also observed in several Al alloys processed by both ECAP and HPT (79, 80). The achievement of a mean grain size of about 100 nm and a large fraction of high-angle GBs after 20 turns of HPT processing was reported in AA7075. The data in **Figure 7** (81) show that clusters approximately 3–5 nm wide are made of GB segregants. Local concentrations up to 25 at. % of Mg in layers of approximately 6–8 nm thick were also observed

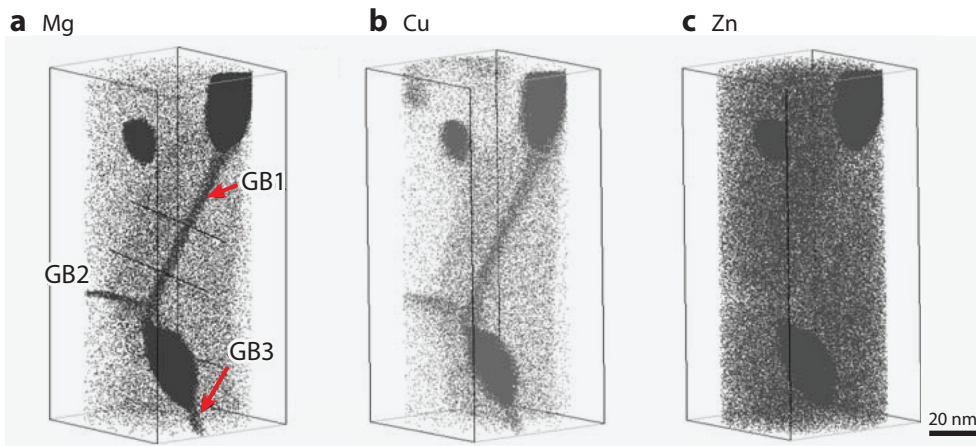


Figure 7

Atom probe tomography elemental maps of a polycrystalline region of an Al-Zn-Mg-Cu alloy after eight passes of equal-channel angular pressing. (a) Mg, (b) Cu, and (c) Zn maps at three grain boundaries (GBs): GB1, GB2, and GB3. Red arrows indicate the position of the GBs. Figure adapted with permission from Reference 82.

by APT (80). It appears, therefore, that nonequilibrium GBs with strain-distorted structure have higher amounts of segregating atoms with respect to relaxed interfaces, and the thickness of the segregated layer may be determined by the distorted layer near the nonequilibrium GB. It follows from APT observations that the distributions of the solute elements may be influenced by the local configurations of the GB, especially dislocations lying at or near the boundaries.

3.4. Nanoparticles and Second-Phase Precipitates

Solution quenching promotes the formation of particles in many alloys subjected to SPD (see, e.g., 17, 83, 84). Examples of such nanoparticles as large as about 10–20 nm precipitated in the UFG Al alloys after ECAP processing are presented in these studies. Nanoparticles appeared due to dynamic aging and caused additional precipitation hardening of the alloys. Parameters of SPD processing usually determine the size and morphology of precipitates. In recent years, the subject of dynamic aging originating from SPD has attracted greater attention because the morphology of precipitates and their formation kinetics differ considerably from the processes of conventional aging and provide for new possibilities in the production of advanced alloys that can be hardened with age (85, 86).

It was recently observed that dynamic aging during HPT competes with dynamic dissolution of precipitates in Cu-based alloys (87). As a result of this competition, a certain steady state forms between dynamic aging and dynamic dissolution (88). This is controlled by an accelerated diffusion-like mass transfer between matrix solid solution and precipitates. As a result of this dynamic equilibrium, a certain steady-state solute concentration is established.

4. NANOSTRUCTURAL DESIGN OF ULTRAFINE-GRAINED MATERIALS THROUGH SPD PROCESSING

As shown in Section 3, unique structural characteristics result from nanostructuring of bulk materials by SPD. Among them are ultrafine grain sizes and shapes; high density of interfaces and lattice defects in the grain interior; and complex structure of GBs, nanotwins, segregation, and second-phase nanoparticles. These nanostructural features can strongly influence transport

and deformation mechanisms, thereby changing the properties of not only metallic materials but also some polymers and ceramics (3, 12, 13).

Deformation mechanisms in nanometals are significantly influenced by GBs, which constitute a large volume fraction in UFG metals. In general, GB-mediated deformation mechanisms can be divided into two basic categories: (a) pure GB mechanisms related to GB sliding and migration and (b) GB-mediated mechanisms associated with twinning and dislocation emission from GBs (12, 13, 69). The pure GB mechanisms include GB sliding, stress-driven GB migration, grain rotations mediated by GB dislocations, and GB and triple-junction diffusional creep. These mechanisms can significantly contribute to plastic deformation in metallic nanograined materials. Both deformation mechanisms depend on the crystallography of GBs and their defect structure related to the presence of GB dislocations and vacancies. In turn, as discussed in Section 3, the GB structure is determined by SPD processing conditions and regimes.

Computer simulation (89) and experimental studies (90, 91) have substantiated the recent discovery of the influence of GB segregation on GB sliding and diffusion in aluminum alloys. Zn segregation at GBs significantly accelerates the diffusion kinetics and sliding, while Mg segregation inhibits this process. This opens the way to control the mechanical properties of nanomaterials and their thermal stability through GB engineering (16, 70, 73, 91).

We now consider some examples of nanostructural design of metals and alloys for enhancement of their mechanical and functional properties. These problems refer specifically to simultaneously improving properties of multifunctional materials that are usually mutually exclusive (12, 17).

4.1. Superior Strength and Ductility

Earlier work on SPD processing (1, 2) focused mainly on grain refinement to improve the mechanical strength of metallic materials according to the well-known Hall–Petch relationship,

$$\sigma_y = \sigma_0 + K_{\text{HP}}d^{-\frac{1}{2}}, \quad 1.$$

where σ_y is the yield stress, d is the grain size, and σ_0 and K_{HP} are constants for a given material. Later, it was revealed that this relationship may break down for nanomaterials with a grain size of <20–50 nm (13). Nevertheless, the Hall–Petch law is usually valid for UFG materials produced by SPD, as they generally have grain sizes in the submicrometer range. The mechanical strength of pure metals can be enhanced by a factor of about 3–6 due to extreme grain refinement via SPD (92, 93). However, as noted above, the SPD-processed materials often have various nanoscale features that provide additional strengthening. The contribution of other strengthening mechanisms (e.g., dislocation hardening, precipitation hardening) can further enhance mechanical strength, resulting in values that are much higher than those predicted by the standard Hall–Petch relationship (92, 94). Such observations of superstrength have been demonstrated for several Al alloys (such as Al 1570 and Al 7475), Ti-6Al-4V, and steels and have already been considered in detail in the literature (12, 92).

GB segregation can provide additional strengthening. Experimental studies of a high-strength UFG Al 1570 alloy, using an APT technique, demonstrated a clear relationship between Mg segregation at GBs and strength (80). Similar observations were also recently reported for several UFG Al alloys and stainless steels (79, 95, 96). A physical explanation for such segregation strengthening is related to dislocations generated at GBs (80). The emitted dislocation glides through the grain interior and is trapped by the opposite GB so that a dislocation–GB interaction plays the role of the rate-controlling mechanism. GB segregation can suppress the emission of dislocations due to a solute drag effect that, in turn, results in higher values of stress required for the dislocation emission. Thus, a new strengthening mechanism related to GB segregation can be observed

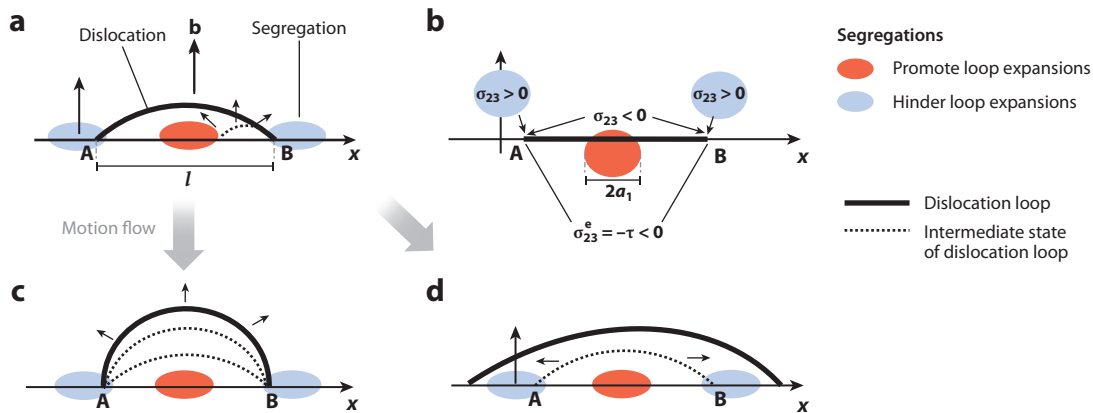


Figure 8

Expansion of a dislocation loop in the presence of segregation. The blue and red ovals denote the segregations that hinder and promote loop expansion, respectively. (a,b) The ends (A and B) of the dislocation loop, which nucleates and expands under the action of the applied load, are pinned by segregation. (a) Projection on the dislocation glide plane illustrates segregation-induced pinning. (b) Projection on the grain boundary plane illustrates the fact that segregation can either promote or hinder dislocation loop expansion, depending on whether pinning is strong or weak. (c) By increasing the applied load, dislocation loop expansion is realized via its bow-out if segregation-induced pinning is strong. (d) If pinning is weak, loop expansion is realized via the unpinning and lateral motion of points A and B. Figure adapted with permission from Reference 97.

in SPD-processed UFG—referred to as GB segregation hardening (16). A model of this process has been recently considered (97). **Figure 8** illustrates the expansion of a dislocation loop in the presence of segregation.

Ductility is required to enable metal-forming operations as well as to avoid catastrophic failure during service. The maximum strain of homogeneous plastic flow before the onset of necking represents the uniform elongation, which is determined by the resistance of the material to macrolocalization of plastic flow (13, 93). This parameter can be useful for determining the ability of material to undergo stretch metal-forming operations. Another parameter determining ductility is the elongation to failure. This parameter takes into account the necking elongation, which is controlled by a competition between localized plastic flow and fracture. Typically, the total elongation of coarse-grained materials is slightly higher than their uniform elongation. For UFG metallic materials, the difference between these two parameters may become very significant. Thus, it is important when analyzing the ductility of UFG metals to unambiguously indicate the precise measure of ductility.

Strength and ductility are the key mechanical properties of any material, but these properties are typically mutually exclusive, such that materials may be strong or ductile but are rarely both. Earlier works focusing on mechanical properties of SPD-processed materials demonstrated that grain refinement down to the nanoscale leads to very high mechanical strength but that these materials invariably exhibit low tensile ductility (98, 99). This problem was well known in metals subjected to heavy straining by processes such as rolling, extrusion, or drawing. The reason for this is that the plastic deformation mechanisms associated with the generation and storage of dislocations may not be active in heavily deformed materials during their further tensile straining. Such a situation is typical for SPD-processed materials as well.

Due to the significance of the problem of mechanical behavior of nanomaterials, the so-called paradox of strength and ductility was introduced in the literature (100, 101). Early reports on combinations of extraordinary strength and ductility in some bulk SPD-processed materials

attracted significant attention from the research community, promoting investigations on the development of novel approaches to improve tensile ductility of bulk nanostructured materials. Recent overviews of these research activities are now available (13, 92, 102, 103). Various strategies to improve the low tensile ductility of nanostructured metals and alloys have been proposed. These approaches can be classified into two separate groups: mechanical strategies and microstructural strategies. The mechanical strategies are based on manipulating some mechanical characteristics of the UFG materials, such as strain rate sensitivity, work hardening ability, or both, which can be controlled via testing parameters (temperature, strain rate, or both). The microstructural strategies are based on the concept of microstructural design at the nanoscale.

Among the strategies for ductility enhancement in UFG metals (see, for example, 13, 102) are the development of bimodal microstructures consisting of micro- and nanograins, developing graded nanograined metals or nanotwinned structures, and tailoring of the stacking fault energy via alloying. These strategies focus on increasing the strain hardening rate, which leads to improved uniform elongation during tensile tests. By contrast, several recent GB engineering strategies are intended to increase the strain rate sensitivity by accelerating GB sliding, significantly enhancing the ductility (total elongation). For example, the presence of Zn segregation at GBs in Al alloys with UFG structure sharply accelerates sliding, which leads to a considerable increase in ductility and even superplasticity at room temperature (90). At the same time, by managing the deformation conditions (e.g., temperature, strain rate), it is possible to successfully combine high strength and ductility.

4.2. High Strength and Electrical Conductivity

A new strategy for nanostructural design in Al and Cu alloys for advanced conductors was recently developed (85, 104, 105). In this strategy, the strengthening mechanisms and mechanisms of electrical resistivity are manipulated by grain refinement (down to the submicrometer scale) and dynamic aging during SPD processing. This results in decomposition of the supersaturated solid solution and the formation of second-phase nanoprecipitates in alloys with UFG structure (**Figure 9**). Boundary strengthening and precipitation hardening resulting in superior mechanical strength are characteristic of these UFG microstructures with second-phase nanoprecipitates. At the same time, significantly enhanced electrical conductivity results from the very low content of

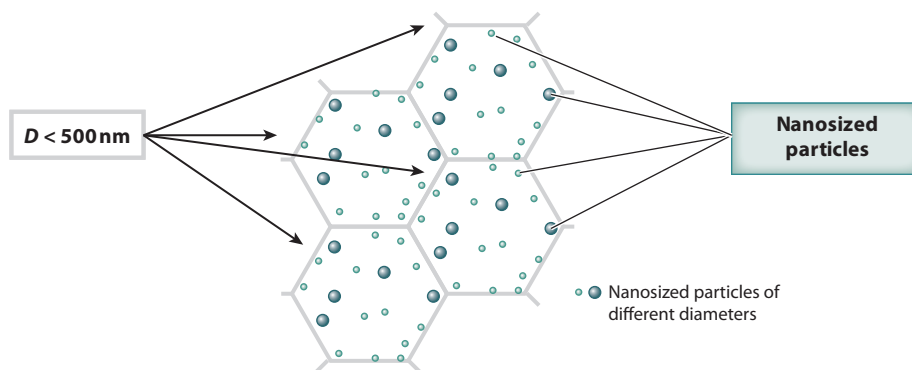


Figure 9

Schematic illustration of nanostructure with nanoparticles to realize the combination of high strength, good electrical conductivity, and enhanced thermal stability in Cu and Al alloys (85). Black arrows indicate average ultrafine grains ($D < 500 \text{ nm}$) (hexagons) and black lines indicate nanosized particles of different diameters. Figure adapted from permission from Reference 104.

solute atoms and the absence of Guinier–Preston zones in the Al matrix. Theoretical evaluations (105) and experimental studies (85, 104) confirm this approach.

The dependence is well described by the ratio for strength (Equation 2) and electrical resistance (Equation 3) that were applied to assess the properties of UFG alloys in References 85, 104, and 105:

$$\sigma_{\text{total}} = \sigma_o + \sigma_{\text{gs}} + \sigma_{\text{ss}} + \sigma_{\text{dis}} + \sigma_{\text{p}}, \quad 2.$$

where σ_o is Peierls stress, σ_{gs} is grain size strengthening, σ_{ss} is solid solution strengthening, σ_{dis} is dislocation strengthening, and σ_{p} is precipitation strengthening.

The effective resistivity of an alloy, ρ , following Matthiessen's rule, is normally written as

$$\rho = \rho_{\text{T}} + \rho_{\text{D}}, \quad 3.$$

where ρ_{T} is a temperature-dependent phonon contribution and ρ_{D} is a contribution from the lattice defects and solutes and is independent of temperature. The temperature-independent part describes resistivity from various defects and thus can be split up into several contributions as

$$\rho_{\text{total}} = \rho_{\text{ss}} + \rho_{\text{p}} + \rho_{\text{dis}} + \rho_{\text{v}} + \rho_{\text{gb}}, \quad 4.$$

where ρ_{ss} is the resistivity due to scattering by solute atoms dissolved in the matrix; ρ_{p} is the resistivity added by second-phase particles; ρ_{dis} and ρ_{v} are resistivity due to dislocations and vacancies, respectively; and ρ_{gb} is the resistivity due to scattering on GBs.

For example, AA6201, an alloy widely used for electroconductors, was chosen for experimental confirmation (85). Disks with diameters of 20 mm and thicknesses of 1.5 mm were solution heat treated at 530°C for 2 h and water quenched. Then, HPT was used for SPD processing of the disks. A strong decomposition of the supersaturated solid solution, confirmed by a significant decrease in the lattice parameter of the Al matrix, was revealed by X-ray diffraction. A good match of the X-ray results with recent APT was revealed (105). Dynamic aging leads to a near-complete purification of the matrix from the solute atoms and formation of 10- to 30-nm spherical nanoprecipitates. The strength and electrical conductivity calculations based on the obtained structural data are in good agreement with the experimental values (105).

4.3. Metallic Biomaterials with Superior Strength and Functionality

Nanostructuring of biocompatible metallic materials by SPD opens up new avenues for their applications in biomedical engineering (38, 106). The most impressive results in this area were achieved for commercially pure Ti. Ti is recognized as one of the most bioinert metals, which makes it attractive for producing medical implants (107, 108). Unlike many Ti alloys, it does not contain any toxic elements. In terms of biocorrosion resistance, Ti is superior to most surgical metals due to the formation of a very stable passive layer of TiO_2 on its surface. Another favorable property of Ti is its low elastic modulus (half that of stainless steel and Co–Cr alloys), which results in less stress shielding and associated bone resorption around Ti orthopedic and dental implants. Furthermore, Ti is lighter than other surgical metals and produces fewer artifacts during computed tomography and magnetic resonance imaging. However, the static and fatigue strengths of commercially pure Ti are too low for it to be used in some load-bearing medical applications. For example, small plates and screws are often used in the maxillofacial area of a skull (109). However, depending on the injury type and locality of bone fixation, loads on implants can vary from 200 to 700 N. The maximum load for a 1-mm-diameter screw can create stresses as high as 900 MPa, which are significantly beyond the ultimate tensile strength (UTS) of commercially pure Ti and require using stronger Ti alloys or stainless steels.

Recent studies have shown that the application of SPD processing techniques such as ECAP-C with a subsequent drawing of the material is the most effective way to produce long-length rods with nanoscale structures (38, 110). Nanostructuring of Ti increases its strength and fatigue resistance to levels that exceed those reported for Ti-6Al-4V ELI alloy (110, 111). The UTS in Ti after ECAP plus drawing is almost twice the value in the initial state after hot rolling. The strength becomes even higher when the degree of straining during drawing is increased without any dramatic reduction of ductility. This is in contrast to conventional deformation processing, such as rolling, extrusion, or drawing, when increasing accumulated strain and microstructure refinement results in strengthening but a concomitant reduction in ductility. This is because these processing techniques result in a subgrain type of microstructure characterized by pronounced metallographic and crystallographic textures as well as high volumes of low-angle GBs. High strength with retained ductility allows the miniaturization of load-bearing implants made from the nanostructured Ti. Miniaturized Ti dental implants (112) and miniplates have been designed using these principles (113).

4.3.1. Nano-Ti dental implants. The reduced diameter of nano-Ti implants allows a reduction in damage during their insertion into the jaw, thus making implantation a less traumatic procedure for the patient. Another advantage is that these implants could be installed in patients with a thin alveolar bone, where conventional implants cannot be used or additional intervention is required (106, 112). The research to date has shown that implants from nano-Ti also have better biological response, including increased cell survival and enhanced cell adhesion (110, 111). Previously, it was found that the colonization of fibroblasts on the surface of grade 4 Ti increased significantly after nanostructuring and chemical etching (114). Observations of patients in a clinical setting have shown that increasing the biological properties of nano-Ti contributes to the rapid engraftment of the implant, and about 70% of nano-Ti implants could be loaded immediately after inserting. So far, over 7,000 dental implants made from nanostructured grade 4 Ti with diameters of 2.4 and 3.5 mm, as well as several implants with a diameter of 2.0 mm, have been inserted in several clinics in the Czech Republic (**Figure 10**). To date, not a single case of rupture or breakage of nano-Ti implants has been reported. The calculations and experimental results show that using available nanostructured Ti with an UTS of 1,330 MPa makes it possible to securely reduce the diameter of the implant down to 2.0 mm (**Figure 10a**). This enables nano-Ti implants even in the case of alveolar bones narrower than 4.5 mm.

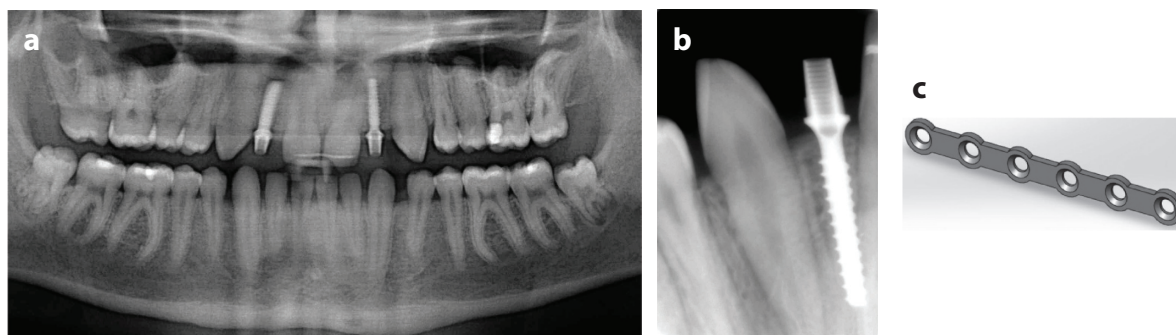


Figure 10

A 2.0-mm-diameter Nanoimplant[®] (<http://www.timplant.cz/en/>) from nanostructured grade 4 Ti in (a) a panoramic X-ray radiograph after surgery and (b) the control radiograph obtained after incorporation of the implant. (c) Image of a miniplate with six holes made from nanostructured grade 4 Ti (110). Panels *a* and *b* reproduced from Reference 115. Panel *c* reproduced from Reference 116.

Table 1 Mechanical properties of conventionally processed and nanostructured grade 4 Ti produced by ECAP-C and drawing

Processing and treatment conditions	UTS (MPa)	YS (MPa)	Elongation (%)	Reduction of area (%)	Fatigue strength at 10 ⁷ cycles (MPa)
Conventional Ti (as received)	700	530	25	52	340
Nano-grade 4	1,330	1,267	11	48	620
Conventional Ti-6Al-4V ELI ^a	940	840	16	45	530

Abbreviations: ECAP-C, equal-channel angular pressing–Conform; ELI, extra low interstitials; UTS, ultimate tensile strength; YS, yield stress.

^aData on Ti-6Al-4V ELI alloy are presented for comparison (110).

4.3.2. Nano-Ti plates for maxillofacial surgery. Using the fatigue endurance limit of conventional and nano-Ti (Table 1), it is possible to design nano-Ti plates with reduced thickness for maxillofacial surgery. Plate thickness can be reduced from 0.9 to 0.7 mm without degradation of its mechanical performance (113). While the standard plates withstood $17,000 \pm 500$ cycles, a nano-Ti plate with reduced cross section withstood $105,000 \pm 800$ cycles (113). This result points to an enhancement of bending strength of the plate from nano-grade 4 Ti despite its reduced thickness, an important advantage over the standard item made from conventional Ti.

4.3.3. Surface modification to improve biointegration. Surface properties are an important aspect of an implant design to ensure effective osseointegration. Pure Ti has very low bioactivity (i.e., it is bioinert) and does not bond directly to the human bone. As a result, the implant may shift and loosen during service life. A significant body of research has shown that grain refinement down to the nanoscale in commercially pure Ti can increase the adhesion and proliferation of various bone-forming cell types (114–121). Additional surface modification can further improve the bioactivity of implants made from UFG Ti, including chemical etching and deposition of bioactive coatings (108, 122–126).

HF-HNO₃-based solutions are used for acid treatment of the implant surface. HF acid interacts with the TiO₂ oxide film and results in the formation of a dense film of fluorides and hydrides. In recent work (126), a mixture of acid etchants was used to reveal the effect of topography of the nano-Ti surface. Nanostructured Ti was found to produce rougher surfaces after etching. Similar results have been reported by numerous researchers (127–129), demonstrating that the specific relief on the nano-Ti surface facilitates higher rates of adhesion for both fibroblast (129) and pre-osteoblast (127) cells.

Biocompatible coatings can facilitate integration of the Ti implants into human bone (130). Therefore, research into synthesis of biocompatible coatings integrating inorganic (e.g., Ca- and P-containing phases) and organic, biologically active components on Ti implants is quite relevant at present (131, 132), with recent results on bioactive coatings on nanostructured biomaterials (133–135).

5. BIODEGRADABLE METALS

Interest is growing in the application of biodegradable metallic materials for manufacturing of devices in the biomedical industry (136, 137). There are strict requirements on reliability, bioresorbability, and biodegradability of materials used for the manufacturing of implants and stents. Nanostructured Mg and Fe can potentially satisfy all these requirements due to their bioresorbability and biodegradability. High strength may be achieved by grain refinement, and corrosion performance can be controlled due to the second-phase particle distributions. The required Young's modulus, the increased possibility of bone adaptation, and a controlled drug release option may be reached by micro- and macroporosity (137, 138).

The high potential of SPD-processed Mg alloys for applications as biodegradable materials was demonstrated in a recent study focused on their biocompatibility (139). Significantly improved mechanical strength and lower corrosion rates without degradation of biocompatibility were observed in an AZ31 Mg alloy after ECAP processing. Acceptable toxicity to MG63 cells with grade I toxicity was demonstrated by the AZ31 Mg alloy after multipass ECAP processing, which was comparable to other standard Mg alloys such as Mg–Ca and Mg–Zn, showing good biocompatibility in in vivo studies. However, a three-pass back-pressure ECAP alloy indicated grade II toxicity, which may be attributed to higher Mg and Al concentrations leading to an osmolarity shock to the cells. Therefore, optimum SPD processing parameters should be selected for fabrication of Mg alloys showing the required mechanical, chemical, and biological properties suitable for biomedical applications. As Mg alloys have a hexagonal close-packed lattice, significant attention must be paid also to the control of crystallographic texture in the ECAP-processed material. The latter provides an extra tool to effectively tune the mechanical properties and resorption rates without reducing cytocompatibility (140–142). Biological properties of the surface can be further enhanced by additional surface modifications (143).

6. SUMMARY AND CONCLUSIONS

The results of this overview provide a clear demonstration that processing by SPD can produce superior properties in bulk nanostructured materials. Based on the evidence available to date, significant information now exists on the underlying mechanisms that account for these special properties, opening new possibilities for practical applications of these materials in novel structural and functional applications. Recent discoveries demonstrate new opportunities for SPD processing for improving other physical and chemical properties of these materials. These properties were mentioned only briefly in this review but nevertheless have achieved considerable advances in recent years (12, 144, 145). These include, for example, increased superconductivity, thermoelectricity, giant magnetoresistance, improved hydrogen storage, and improved biocompatibility.

A general rule in modern materials science is that any material breakthrough in the twentieth century required, from the time of the initial innovation, about two decades to achieve widespread market acceptance (146). It appears that bulk nanostructured metallic materials, as produced by SPD processing, are also following this track. Although the first developments and research started at the beginning of the 1990s, there have been very significant developments in the commercialization of these materials in recent years. This is especially evident from the widespread production of advanced pilot articles with new functionalities (38).

There are three primary advantages associated with the application and commercialization of bulk nanostructured metals: markedly superior properties, the potential for efficient fabrication using SPD processing techniques such as ECAP-C, and the possibility of using these materials to produce cutting-edge products. Furthermore, many of these new applications involve, or will involve, extreme environmental conditions requiring both exceptional strength and improved functional properties.

It is reasonable to anticipate that, in the very near future, the nanostructuring of materials by SPD processing will lead to new breakthroughs in the development of bulk solids with superior properties for advanced structural and functional applications.

DISCLOSURE STATEMENT

The authors are not aware of any affiliations, memberships, funding, or financial holdings that might be perceived as affecting the objectivity of this review.

ACKNOWLEDGMENTS

R.Z.V. gratefully acknowledges financial support from the Russian Science Foundation in the framework of Project No. 20-63-47027 (Section 4.3 on nanostructured Ti for medical applications) and the Ministry of Science and Higher Education of the Russian Federation in the framework of a state assignment (Project No. FSNM-2020-0027) for research in his part of this review. The work of T.G.L. was supported by the European Research Council under Grant Agreement No. 267464-SPDMETALS. We are especially grateful to all who provided support, comments, and fruitful discussions and allowed us to cite their publications during the work on this review, in particular colleagues from the Institute of Physics of Advanced Materials, Ufa State Aviation Technical University, and the Laboratory for Mechanics of Advanced Nanomaterials, Saint-Petersburg State University, for jointly obtained results. We especially thank our colleagues and friends from the International NanoSPD Steering Committee for drawing our attention to major new activities in the field of SPD processing. We apologize to all collaborators whose contributions we may have overlooked. However, their comments on this review are always welcome and highly appreciated.

LITERATURE CITED

1. Valiev RZ, Islamgaliev RK, Alexandrov IV. 2000. Bulk nanostructured materials from severe plastic deformation. *Prog. Mater. Sci.* 45:103–89
2. Langdon TG. 2013. Twenty-five years of ultrafine-grained materials: achieving exceptional properties through grain refinement. *Acta Mater.* 61:7035–59
3. Horita Z, Edalati K. 2020. Severe plastic deformation for nanostructure controls. *Mater. Trans.* 61:2241
4. Valiev RZ, Langdon TG. 2006. Principles of equal-channel angular pressing as a processing tool for grain refinement. *Prog. Mater. Sci.* 51:881–981
5. Zhilyaev AP, Langdon TG. 2008. Using high-pressure torsion for metal processing: fundamentals and applications. *Prog. Mater. Sci.* 53:893–979
6. Estrin Y, Vinogradov A. 2013. Extreme grain refinement by severe plastic deformation: a wealth of challenging science. *Acta Mater.* 61:782–817
7. Rosochowski A. 2017. *Severe Plastic Deformation Technology*. Dunbeath, UK: Whittles. 1st ed.
8. Valiev RZ, Estrin Y, Horita Z, Langdon TG, Zehetbauer MJ, Zhu YT. 2006. Producing bulk ultrafine-grained materials by severe plastic deformation. *JOM* 58(4):33–39
9. Beyerlein IJ, Toth LS. 2009. Texture evolution in equal-channel angular extrusion. *Prog. Mater. Sci.* 54:427–510
10. Zehetbauer MJ, Zhu YT, eds. 2009. *Bulk Nanostructured Materials*. Weinheim, Ger.: Wiley
11. Bachmaier A, Pippan R. 2013. Generation of metallic nanocomposites by severe plastic deformation. *Int. Mater. Rev.* 58:41–62
12. Valiev RZ, Estrin Y, Horita Z, Langdon TG, Zehetbauer MJ, Zhu YT. 2016. Fundamentals of superior properties in bulk nanoSPD materials. *Mater. Res. Lett.* 4:1–21
13. Ovid'ko IA, Valiev RZ, Zhu YT. 2018. Review on superior strength and enhanced ductility of metallic nanomaterials. *Progress Mater. Sci.* 94:462–540
14. Straumal BB, Kilmametov AR, Ivanisenko Yu, Mazilkin AA, Kogtenkova OA, et al. 2015. Phase transitions induced by severe plastic deformation: steady-state and equifinality. *Int. J. Mater. Res.* 106:657–64
15. Andrievski RA, Glezer AM. 2009. Strength of nanostructures. *Phys.-Uspekhi* 52(4):315–34
16. Valiev RZ, Zhilyaev AP, Langdon TG. 2014. *Bulk Nanostructured Materials: Fundamentals and Applications*. Hoboken, NJ: Wiley
17. Sabirov I, Enikeev NA, Murashkin MYu, Valiev RZ. 2015. *Bulk Nanostructured Materials with Multifunctional Properties*. Cham, Switz.: Springer
18. Sauvage X, Wilde G, Divinski SV, Horita Z, Valiev RZ. 2012. Grain boundaries in ultrafine grained materials processed by severe plastic deformation and related phenomena. *Mater. Sci. Eng. A* 540:1–12
19. Straumal BB, Kilmametov AR, López-Ferreño I, N6 ML, et al. 2017. High-pressure torsion driven phase transformations in Cu-Al-Ni shape memory alloys. *Acta Mater.* 125:274–85

20. Kilmametov AR, Ivanisenko Yu, Mazilkin AA, Straumal BB, Gornakova AS, et al. 2018. The $\alpha \rightarrow \omega$ and $\beta \rightarrow \omega$ phase transformations in Ti–Fe alloys under high-pressure torsion. *Acta Mater.* 144:337–51
21. Edalati K, Horita Z. 2010. Continuous high-pressure torsion. *J. Mater. Sci.* 45:4578–82
22. Xu C, Schroeder S, Berbon PB, Langdon TG. 2010. Principles of ECAP–Conform as a continuous process for achieving grain refinement: application to an aluminium alloy. *Acta Mater.* 58:1379–86
23. Mishnaevsky L Jr., Levashov E, Valiev RZ, Segurado J, Sabirov I, et al. 2014. Nanostructured titanium-based materials for medical implants: modeling and development. *Mater. Sci. Eng. R.* 81:1–19
24. Faraji G, Torabzadeh H. 2019. An overview on the continuous severe plastic deformation methods. *Mater. Trans.* 60(7):1316–30
25. Edalati K, Horita Z. 2016. A review on high-pressure torsion (HPT) from 1935 to 1988. *Mater. Sci. Eng. A* 652:325–52
26. Bridgman PW. 1935. Effects of high shearing stress combined with high hydrostatic pressure. *Phys. Rev.* 48:825–47
27. Valiev RZ, Kaibyshev OA, Kuznetsov RI, Musalimov RSh, Tsenev NK. 1988. Low-temperature superplasticity of metallic materials. *Dokl. Akad. Nauk. SSSR* [Rep. USSR Acad. Sci.] 301(4):864–66
28. Lowe TC, Valiev RZ, eds. 2000. *Investigations and Applications of Severe Plastic Deformation*. Dordrecht, Neth.: Kluwer Acad.
29. Valiev RZ, Tsenev NK. 1991. Simulation of the spectrum of grain-boundary orientation in polycrystals with a crystallographic texture. In *Hot Deformation of Aluminium Alloys*, ed. TG Langdon, HD Merchant, JG Morris, MA Zaidi, pp. 319–23. Warrendale, PA: Miner. Met. Mater. Soc.
30. Zhu YT, Valiev RZ, Langdon TG, Tsuji N, Lu K. 2010. Processing of nanostructured metals and alloys via plastic deformation. *MRS Bull.* 35:977–81
31. Whang SH, ed. 2011. *Nanostructured Metals and Alloys: Processing, Microstructure, Mechanical Properties and Applications*. Cambridge, UK: Woodhead
32. Rosochowski A, Olejnik L. 2011. Incremental equal channel angular pressing for grain refinement. *Mater. Sci. Forum.* 674:19–28
33. Gzyl M, Rosochowski A, Boczkal S, Olejnik L. 2015. The role of microstructure and texture in controlling mechanical properties of AZ31B magnesium alloy processed by I-ECAP. *Mater. Sci. Eng. A* 638:20–29
34. Segal VM, Reznikov VI, Kopylov VI, Pavlik DA, Malyshev VF. 1994. *Processes of Structure Evolution by Plastic Deformation in Metals*. Minsk, Belarus: Nauk. Tekhnika
35. Raab GI, Valiev RZ, Lowe TC, Zhu YT. 2004. Continuous processing of ultrafine grained Al by ECAP–Conform. *Mater. Sci. Eng. A* 382:30–34
36. Ayati V, Parsa MH, Mirzadeh H. 2015. Deformation of pure aluminum along the groove path of ECAP–Conform process. *Adv. Eng. Mater.* 18:319–23
37. Duchek M, Kubina T, Hodek J, Dlouhy J. 2013. Development of the production of ultra-fine grained titanium with the conform equipment. *Mater. Technol.* 47:515–18
38. Lowe TC, Valiev RZ, Li X, Ewing B. 2021. Commercialization of bulk nanostructured metals and alloys. *MRS Bull.* 46:265–72
39. Murashkin MYu, Medvedev A, Kazykhanov V, Krokhin A, Raab GI, et al. 2015. Enhanced mechanical properties and electrical conductivity in ultrafine-grained Al 6101 alloy processed via ECAP–Conform. *Metals* 5:2148–64
40. Harai Y, Edalati K, Horita Z, Langdon TG. 2009. Using ring samples to evaluate the processing characteristics in high-pressure torsion. *Acta Mater.* 57:1147–53
41. Edalati K, Horita Z. 2009. Scaling-up of high pressure torsion using ring shape. *Mater. Trans.* 50:92–95
42. Fujioka T, Horita Z. 2009. Development of high-pressure sliding process for microstructural refinement of rectangular metallic sheets. *Mater. Trans.* 50:930–33
43. Edalati K, Lee S, Horita Z. 2012. Continuous high-pressure torsion using wires. *J. Mater. Sci.* 47:473–78
44. Hohenwarter A. 2015. Incremental high pressure torsion as a novel severe plastic deformation process: processing features and application to copper. *Mater. Sci. Eng. A* 626:80–85
45. Stolyarov VV, Zhu YT, Lowe TC, Islamgaliev RK, Valiev RZ. 1999. A two step SPD processing of ultrafine-grained titanium. *Nanostr. Mater.* 11:947–54

46. Zhilyaev AP, Langdon TG. 2012. Microstructure and microtexture evolution in pure metals after ultra-high straining. *J. Mater. Sci.* 47:7888–93
47. Zhang P, An XH, Zhang ZJ, Wu SD, Li SX, et al. 2012. Optimizing strength and ductility of Cu-Zn alloys through severe plastic deformation. *Scr. Mater.* 67:871–74
48. Lugo N, Llorca N, Cabrera JM, Horita Z. 2008. Microstructures and mechanical properties of pure copper deformed severely by equal-channel angular pressing and high pressure torsion. *Mater. Sci. Eng. A* 477:366–71
49. Skiba J, Dominiak A, Wiśniewski TS, Pachla W, Kulczyk M, Przybysz S. 2015. Influence of severe plastic deformation induced by HE and ECAP on the thermo-physical properties of metals. *Key Eng. Mater.* 641:278–85
50. Asselli AAC, Leiva DR, Huot J, Kawasaki M, Langdon TG, Botta WJ. 2015. Effects of equal-channel angular pressing and accumulative roll-bonding on hydrogen storage properties of a commercial ZK60 magnesium alloy. *Int. J. Hydrog. Energy* 40:16971–76
51. Murashkin MYu, Enikeev NA, Kazykhanov VU, Sabirov I, Valiev RZ. 2013. Physical simulation of cold rolling of ultra-fine grained Al5083 alloy to study microstructure evolution. *Rev. Adv. Mater. Sci.* 35:75–85
52. Lima GF, Triques MRM, Kiminami CS, Botta WJ, Jorge AM Jr. 2014. Hydrogen storage properties of pure Mg after the combined processes of ECAP and cold-rolling. *J. Alloy. Compd.* 586:S405–8
53. Polyakov AV, Semenova IP, Huang Y, Valiev RZ, Langdon TG. 2014. Fatigue life and failure characteristics of an ultrafine-grained Ti-6Al-4V alloy processed by ECAP and extrusion. *Adv. Eng. Mater.* 16:1038–43
54. Sabirov I, Perez-Prado MT, Molina-Aldareguia JM, Semenova IP, Salimgareeva GK, Valiev RZ. 2011. Anisotropy of mechanical properties in high-strength ultra-fine-grained pure Ti processed via a complex severe plastic deformation route. *Scr. Mater.* 64:69–72
55. Gubicza J, Fogarassy Zs, Krállics Gy, Lábár J, Törkölly T. 2008. Microstructure and mechanical behavior of ultrafine-grained titanium. *Mater. Sci. Forum.* 589:99–104
56. Stepanov ND, Kuznetsov AV, Salishchev GA, Raab GI, Valiev RZ. 2012. Effect of cold rolling on microstructure and mechanical properties of copper subjected to ECAP with various numbers of passes. *Mater. Sci. Eng. A* 554:105–15
57. Fan Z, Jiang H, Sun X, Song J, Zhang X, Xie C. 2009. Microstructures and mechanical deformation behaviors of ultrafine-grained commercial pure (grade 3) Ti processed by two-step severe plastic deformation. *Mater. Sci. Eng. A* 527:45–51
58. Sordi VL, Ferrante M, Kawasaki M, Langdon TG. 2012. Microstructure and tensile strength of grade 2 titanium processed by equal-channel angular pressing and by rolling. *J. Mater. Sci.* 47:7870–76
59. Latysh VV, Semenova IP, Salimgareeva GH, Kandarov IV, Zhu YT, et al. 2006. Microstructure and properties of Ti rods produced by multi-step SPD. *Mater. Sci. Forum.* 503–504:763–68
60. Ferguson D, Chen W, Bonesteel T, Vosburgh J. 2009. A look at physical simulation of metallurgical processes, past, present and future. *Mater. Sci. Eng. A* 499:329–32
61. Ivanisenko Yu, Kulagin R, Fedorov V, Mazilkin A, Scherer T, et al. 2016. High pressure torsion extrusion as a new severe plastic deformation process. *Mater. Sci. Eng. A* 664:247–56
62. Kilmametov A, Ivanisenko Yu, Straumal BB, Mazilkin AA, Gornakova AS, et al. 2017. Transformations of α' martensite in Ti-Fe alloys under high pressure torsion. *Scr. Mater.* 136:46–49
63. Gleiter H. 1989. Nanocrystalline materials. *Prog. Mater. Sci.* 33:223–315
64. Gleiter H. 2000. Nanostructured materials: basic concepts and microstructure. *Acta Mater.* 48:1–29
65. McKenzie PWJ, Lapovok R. 2010. ECAP with back pressure for optimum strength and ductility in aluminium alloy 6016. Part 1: microstructure. *Acta Mater.* 58(9):3198–211
66. Renk O, Pippan R. 2019. Saturation of grain refinement during severe plastic deformation of single phase materials: reconsiderations, current status and open questions. *Mater. Trans.* 60(7):1270–82
67. Kolobov YR, Grabovetskaya GP, Ivanov KV, Ivanov MB. 2002. Grain boundary diffusion and mechanisms of creep of nanostructured metals. *Interface Sci.* 10(1):31–36
68. Divinski SV, Reglitz G, Rösner H, Wilde G, Estrin Y. 2011. Self-diffusion in Ni prepared by severe plastic deformation: effect of non-equilibrium grain boundary state. *Acta Mater.* 59:1974–85

69. Wilde G, Divinski S. 2019. Grain boundaries and diffusion phenomena in severely deformed materials. *Mater. Trans.* 60(7):1302–15
70. Raabe D, Herbig M, Sandlöbes S, Li Y, Tytko D, et al. 2014. Grain boundary segregation engineering in metallic alloys: a pathway to the design of interfaces. *Curr. Opin. Solid State Mater. Sci.* 18:253–61
71. Horita Z, Smith DJ, Furukawa M, Nemoto M, Valiev RZ, Langdon TG. 1996. An investigation of grain boundaries in submicrometer-grained Al-Mg solid solution alloys using high-resolution electron microscopy. *J. Mater. Res.* 11:1880–90
72. Wang J, Horita Z, Furukawa M, Nemoto M, Tsenev NK, et al. 1993. An investigation of ductility and microstructural evolution in an Al-3% Mg alloy with submicron grain size. *J. Mater. Res.* 8:2810–18
73. Schuh A, Lu K. 2021. Stability of nanocrystalline metals: the role of grain-boundary chemistry and structure. *MRS Bull.* 46:225–35
74. Zhu YT, Liao XZ, Wu XL. 2012. Deformation twinning in nanocrystalline materials. *Prog. Mater. Sci.* 57:1–62
75. Zhao Y, Bingert JF, Liao X, Cui B, Han K, et al. 2006. Simultaneously increasing the ductility and strength of ultra-fine-grained pure copper. *Adv. Mater.* 18:2949–53
76. Lu K, Lu L, Suresh S. 2009. Strengthening materials by engineering coherent internal boundaries at the nanoscale. *Science* 324:349–52
77. Straumal BB, Kogtenkova OA, Gornakova AS, Sursaeva VG, Baretzky B. 2016. Review: grain boundary faceting-roughening phenomena. *J. Mater. Sci.* 51:382–404
78. Nurislamova GV, Sauvage X, Murashkin MYu, Islamgaliev RK, Valiev RZ. 2008. Nanostructure and related mechanical properties of an Al-Mg-Si alloy processed by severe plastic deformation. *Phil. Mag. Lett.* 88:459–66
79. Liddicoat PV, Liao X-Z, Zhao Y, Zhu YT, Murashkin MYu, et al. 2010. Nanostructural hierarchy increases the strength of aluminium alloys. *Nat. Comm.* 1:63
80. Valiev RZ, Enikeev NA, Murashkin MYu, Kazykhanov VU, Sauvage X. 2010. On the origin of extremely high strength of ultrafine-grained Al alloys produced by severe plastic deformation. *Scr. Mater.* 63:949–52
81. Sha G, Yao L, Liao X, Ringer SP, Duan ZC, Langdon TG. 2011. Segregation of solute elements at grain boundaries in an ultrafine grained Al-An-Mg-Cu alloy. *Ultramicroscopy* 111:500–5
82. Sha G, Ringer SP, Duan ZC, Langdon TG. 2013. An atom probe characterisation of grain boundaries in an aluminium alloy processed by equal-channel angular pressing. *Int. J. Mater. Res.* 100:1674–78
83. Valiev RZ, Murashkin MYu, Bobruk EV, Raab GI. 2009. Grain refinement and mechanical behavior of the Al alloy, subjected to the new SPD technique. *Mater. Trans.* 50:87–91
84. Cheng S, Zhao YH, Zhu YT, Ma E. 2007. Optimizing the strength and ductility of fine structured 2024 Al alloy by nano-precipitation. *Acta Mater.* 55:5822–32
85. Valiev RZ, Murashkin MYu, Sabirov I. 2014. A nanostructural design to produce high strength Al alloys with enhanced electrical conductivity. *Scr. Mater.* 76:13–16
86. Ma K, Zheng Y, Dasari S, Zhang D, Fraser HL, Banerjee R. 2021. Precipitation in nanostructured alloys: a brief review. *MRS Bull.* 46:250–57
87. Straumal BB, Kilmametov AR, Korneva A, Mazilkin AA, Straumal PB, et al. 2017. Phase transitions in Cu-based alloys under high pressure torsion. *J. Alloy. Compd.* 707:20–26
88. Straumal BB, Pontikis V, Kilmametov AR, Mazilkin AA, Dobatkin SV, Baretzky B. 2017. Competition between precipitation and dissolution in Cu-Ag alloys under high pressure torsion. *Acta Mater.* 122:60–71
89. Petrik MV, Kuznetsov AR, Enikeev NA, Gornostyrev YuN, Valiev RZ. 2018. Peculiarities of interactions of alloying elements with grain boundaries and the formation of segregations in Al-Mg and Al-Zn alloys. *Phys. Metal. Metallogr.* 119(10):607–12
90. Edalati K, Horita Z, Valiev RZ. 2018. Transition from poor ductility to room-temperature superplasticity in a nanostructured aluminum alloy. *Sci. Rep.* 8:6740
91. Chinh NQ, Murashkin MYu, Bobruk EV, Labar J, Gubicza J, et al. 2021. Ultralow-temperature superplasticity and its novel mechanism in ultrafine-grained Al alloys. *Mater. Res. Lett.* 9:475–82
92. Valiev RZ, Zhu YT. 2015. Recent findings in superior strength and ductility of ultrafine-grained materials. *Trans. Mater. Res. Soc. Jpn.* 40:309–18

93. Balasubramanian N, Langdon TG. 2016. The strength–grain size relationship in ultrafine-grained metals. *Metall. Mater. Trans. A* 47:5827–38
94. Valiev RZ, Enikeev NA, Langdon TG. 2011. Towards superstrength of nanostructured metals and alloys produced by SPD. *Kovov. Mater.* 49:1–9
95. Abramova MM, Enikeev NA, Valiev RZ, Etienne A, Radiguet B, et al. 2014. Grain boundary segregation induced strengthening of an ultrafine-grained austenitic stainless steel. *Mater. Lett.* 136:349–52
96. Scheriau S, Zhang Z, Kleber S, Pippin R. 2011. Deformation mechanisms of a modified 316L austenitic steel subjected to high pressure torsion. *Mater. Sci. Eng. A* 528:2776–86
97. Bobylev SV, Enikeev NA, Sheinerman AG, Valiev RZ. 2019. Strength enhancement induced by grain boundary solute segregations in ultrafine-grained alloys. *Int. J. Plast.* 123:133–44
98. Zhu YT, Han BQ, Lavernia EJ. 2009. Deformation mechanisms of nanostructured materials. In *Bulk Nanostructured Materials*, ed. MJ Zehetbauer, YT Zhu, pp. 89–108. Weinheim, Ger.: Wiley
99. Koch CC. 2009. Nanostructured materials: an overview. In *Bulk Nanostructured Materials*, ed. MJ Zehetbauer, YT Zhu, pp. 3–20. Weinheim, Ger.: Wiley
100. Valiev RZ. 2004. Nanostructuring of metals by severe plastic deformation for advanced properties. *Nat. Mater.* 3:511–16
101. Valiev RZ, Alexandrov IV, Zhu YT, Lowe TC. 2002. Paradox of strength and ductility in metals processed by severe plastic deformation. *J. Mater. Res.* 17:5–8
102. Kumar P, Kawasaki M, Langdon TG. 2016. Review: overcoming the paradox of strength and ductility in ultrafine-grained materials at low temperatures. *J. Mater. Sci.* 51:7–18
103. Alawadhi MY, Sabbaghianrad S, Huang Y, Langdon TG. 2021. Evaluating the paradox of strength and ductility in ultrafine-grained oxygen-free copper processed by ECAP at room temperature. *Mater. Sci. Eng. A* 802:140546
104. Islamgaliev RK, Nesterov KM, Bourgon J, Champion Y, Valiev RZ. 2014. Nanostructured Cu-Cr alloy with high strength and electrical conductivity. *J. Appl. Phys.* 115:194301
105. Murashkin MYu, Sabirov I, Sauvage X, Valiev RZ. 2016. Nanostructured Al and Cu alloys with superior strength and electrical conductivity. *J. Mater. Sci.* 51:33–49
106. Lowe TC, Valiev RZ. 2014. Frontiers of bulk nanostructured metals in biomedical applications. In *Advanced Biomaterials and Biodevices*, ed. A Tiwari, AN Nordin, pp. 3–52. Hoboken, NJ: Wiley-Scrivener
107. Brunette DM, Tengvall P, Textor M, Thomsen P. 2001. *Titanium in Medicine*. Berlin: Springer-Verlag
108. Froes FH, Qian M, eds. 2018. *Titanium in Medical and Dental Applications*. Duxford, UK: Woodhead. 1st ed.
109. Geetha M, Singh AK, Asokamani R, Gogia AK. 2009. Ti based biomaterials, the ultimate choice for orthopaedic implants – a review. *Prog. Mater. Sci.* 54:397–425
110. Valiev RZ, Sabirov I, Zemtsova EG, Parfenov EV, Dluhoš L, Lowe TC. 2018. Nanostructured commercially pure Ti for development of miniaturized biomedical implants. In *Titanium in Medical and Dental Applications*, ed. FH Froes, M Qian, pp. 393–417. Duxford, UK: Woodhead. 1st ed.
111. Valiev RZ, Semenova IP, Latysh VV, Rack H, Lowe TC, et al. 2008. Nanostructured titanium for biomedical applications. *Adv. Eng. Mater.* 10(8):B15–17
112. Polyakov AV, Dyakonov GS, Semenova IP, Raab GI, Dluhos L, Valiev RZ. 2015. Development and study of medical implants made from nanostructured titanium. *Adv. Biomat. Dev. Med.* 2:63–69
113. Semenova IP, Klevtsov GV, Klevtsova NA, Dyakonov GS, Matchin AA, Valiev RZ. 2016. Nanostructured titanium for maxillofacial mini-implants. *Adv. Eng. Mater.* 18(7):1216–24
114. Estrin Y, Ivanova EP, Michalska A, Truong VK, Lapovok R, Boyd R. 2011. Accelerated stem cell attachment to ultrafine grained titanium. *Acta Biomater.* 7:900–6
115. Polyakov AV, Dluhoš L, Dyakonov GS, Raab GI, Valiev RZ. 2015. Recent advances in processing and application of nanostructured titanium for dental implants. *Adv. Eng. Mater.* 17:1869–75
116. Valiev RZ, Parfenov EV, Parfenova LV. 2019. Developing nanostructured metals for manufacturing of medical implants with improved design and biofunctionality. *Mater. Trans.* 60:1356–66
117. An B, Li Z, Diao X, Xin H, Zhang Q, et al. 2016. In vitro and in vivo studies of ultrafine-grain Ti as dental implant material processed by ECAP. *Mater. Sci. Eng. C* 67:34–41
118. Bagherifard S, Ghelichi R, Khademhosseini A, Guagliano M. 2014. Cell response to nanocrystallized metallic substrates obtained through severe plastic deformation. *ACS Appl. Mater. Interfaces* 6:7963–85

119. Park JW, Kim YJ, Park CH, Lee DH, Ko YG, et al. 2009. Enhanced osteoblast response to an equal channel angular pressing-processed pure titanium substrate with microrough surface topography. *Acta Biomater.* 5:3272–80
120. Lai M, Cai K, Hu Y, Yang X, Liu Q. 2012. Regulation of the behaviors of mesenchymal stem cells by surface nanostructured titanium. *Colloids Surf. B Biointerfaces* 97:211–20
121. Nie FL, Zheng YF, Wei SC, Wang DS, Yu ZT, et al. 2013. In vitro and in vivo studies on nanocrystalline Ti fabricated by equal channel angular pressing with microcrystalline CP Ti as control. *J. Biomed. Mater. Res. Part A* 101A:1694–707
122. Elias CN. 2010. Titanium dental implant surfaces. *Rev. Mater.* 15:138–42
123. Liu X, Chu PK, Ding C. 2004. Surface modification of titanium, titanium alloys, and related materials for biomedical applications. *Mater. Sci. Eng. R.* 47:49–121
124. Yao ZQ, Ivanisenko Yu, Diemant T, Caron A, Chuvilin A, et al. 2010. Synthesis and properties of hydroxyapatite-containing porous titania coating on ultrafine-grained titanium by micro-arc oxidation. *Acta Biomater.* 6:2816–25
125. Zemtsova EG, Arbenin AY, Valiev RZ, Orekhov EV, Semenov VG, Smirnov VM. 2016. Two-level micro-to-nanoscale hierarchical TiO₂ nanolayers on titanium surface. *Materials* 9(12):1010
126. Nazarov DV, Zemtsova EG, Valiev RZ, Smirnov VM. 2015. Formation of micro-and nanostructures on the nanotitanium surface by chemical etching and deposition of titania films by atomic layer deposition (ALD). *Materials* 8(12):8366–77
127. Estrin Y, Kasper C, Diederichs S, Lapovok R. 2009. Accelerated growth of preosteoblastic cells on ultrafine grained titanium. *J. Biomed. Mater. Res. A* 90:1239–42
128. Faghihi S, Zhilyaev AP, Szpunar JA, Azari F, Vali H, Tabrizian M. 2007. Nanostructuring of a titanium material by high-pressure torsion improves pre-osteoblast attachment. *Adv. Mater.* 19:1069–73
129. Kim TN, Balakrishnan A, Lee BC, Kim WS, Dvorankova B, et al. 2008. In vitro fibroblast response to ultra fine grained titanium produced by a severe plastic deformation process. *J. Mater. Sci. Mater. Med.* 19:553–57
130. Zhang BGX, Myers DE, Wallace GW, Brandt M, Choong PFM. 2014. Bioactive coatings for orthopaedic implants—recent trends in development of implant coatings. *Int. J. Mol. Sci.* 15:11878–921
131. Dorozhkin SV. 2015. Calcium orthophosphate deposits: preparation, properties and biomedical applications. *Mater. Sci. Eng. C* 55:272–326
132. Lugovskoy A, Lugovskoy S. 2014. Production of hydroxyapatite layers on the plasma electrolytically oxidized surface of titanium alloys. *Mater. Sci. Eng. C* 43:527–32
133. Parfenov E, Parfenova L, Mukaeva V, Farrakhov R, Stotskiy A, et al. 2020. Biofunctionalization of PEO coatings on titanium implants with inorganic and organic substances. *Surf. Coat. Technol.* 404:126486
134. Valiev RZ, Parfenov EV, Parfenova LV. 2019. Developing nanostructured metals for manufacturing of medical implants with improved design and biofunctionality. *Mater. Trans.* 60(7):1356–66
135. Balasubramanian R, Nagumothu R, Parfenov E, Valiev R. 2021. Development of nanostructured titanium implants for biomedical implants – a short review. *Mater. Today: Proc.* 46:1195–200
136. Li H, Zheng Y, Qin L. 2014. Progress of biodegradable metals. *Prog. Nat. Sci.: Mater. Int.* 24:414–22
137. Zheng YF, Gu XN, Witte F. 2014. Biodegradable metals. *Mater. Sci. Eng. R.* 77:1–34
138. Waizy H, Seitz JM, Reifenrath J, Weizbauer A, Bach FW, et al. 2013. Biodegradable magnesium implants for orthopedic applications. *J. Mater. Sci.* 48:39–50
139. Mostaed E, Hashempour M, Fabrizi A, Dellasega D, Bestetti M, et al. 2014. Microstructure, texture evolution, mechanical properties and corrosion behavior of ECAP processed ZK60 magnesium alloy for biodegradable applications. *J. Mech. Behav. Biomed. Mater.* 37:307–22
140. Dobatkin S, Galkin S, Estrin Y, Serebryany V, Diez M, et al. 2019. Grain refinement, texture, and mechanical properties of a magnesium alloy after radial-shear rolling. *J. Alloy. Compd.* 774:969–79
141. Merson E, Poluyanov V, Myagkikh P, Merson D, Vinogradov A. 2021. Inhibiting stress corrosion cracking by removing corrosion products from the Mg-Zn-Zr alloy pre-exposed to corrosion solutions. *Acta Mater.* 205:116570

142. Parfenov EV, Kulyasova OB, Mukaeva VR, Mingo B, Farrakhov RG, et al. 2020. Influence of ultra-fine grain structure on corrosion behaviour of biodegradable Mg-1Ca alloy. *Corros. Sci.* 163:108303
143. Wang J, Tang J, Zhang P, Li Y, Wang J, et al. 2012. Surface modification of magnesium alloys developed for bioabsorbable orthopedic implants: a general review. *J. Biomed. Mater. Res. B* 100:1691–701
144. Valiev RZ, Estrin Y, Horita Z, Langdon TG, Zehetbauer MJ, Zhu YT. 2016. Producing bulk ultrafine-grained materials by severe plastic deformation: ten years later. *JOM* 68:1216–26
145. Edalati K, Bachmaier A, Beloshenko VA, Beygelzimer Y, Blank VD, et al. 2022. Nanomaterials by severe plastic deformation: review of historical developments and recent advances. *Mater. Res. Lett.* 10(4):163–256
146. Eagar T. 1995. Bringing new materials to market. *Tech. Rev.* 98:42–49

Contents

An Overview for the Design of Antimicrobial Polymers: From Standard Antibiotic-Release Systems to Topographical and Smart Materials <i>Humberto Palza, Belén Barraza, and Felipe Olate-Moya</i>	1
Dynamic Nuclear Polarization Solid-State NMR Spectroscopy for Materials Research <i>Iliia B. Moroz and Michal Leskes</i>	25
Crystalline Cholesterol: The Material and Its Assembly Lines <i>Neta Varsano, Jenny Capua-Shenkar, Leslie Leiserowitz, and Lia Addadi</i>	57
Molecular Magnetism <i>Nicholas F. Chilton</i>	79
Teaching Metal-Organic Frameworks to Conduct: Ion and Electron Transport in Metal-Organic Frameworks <i>Ruby A. Kharod, Justin L. Andrews, and Mircea Dincă</i>	103
Design and Characterization of Host Frameworks for Facile Magnesium Transport <i>Yirong Gao, Tara P. Mishra, Shou-Hang Bo, Gopalakrishnan Sai Gautam, and Pieremanuele Canepa</i>	129
Strain Glass State, Strain Glass Transition, and Controlled Strain Release <i>Dong Wang, Yuanchao Ji, Xiaobing Ren, and Yunzhi Wang</i>	159
Angstrofluidics: Walking to the Limit <i>Yi You, Abdulghani Ismail, Gwang-Hyeon Nam, Solleti Goutham, Ashok Keerthi, and Boya Radha</i>	189
Exothermic Formation Reactions as Local Heat Sources <i>Shane Q. Arlington, Gregory M. Fritz, and Timothy P. Weibs</i>	219
Innovations Toward the Valorization of Plastics Waste <i>Zachary R. Hinton, Michael R. Talley, Pavel A. Kots, Anne V. Le, Tan Zhang, Michael E. Mackay, Aditya M. Kunjapur, Peng Bai, Dionisios G. Vlachos, Mary P. Watson, Michael C. Berg, Thomas H. Epps III, and LaShanda T. Korley</i>	249

Mechanical Properties of Metal Nanolaminates <i>Irene J. Beyerlein, Zezhou Li, and Nathan A. Mara</i>	281
Transport in Lithium Garnet Oxides as Revealed by Atomistic Simulations <i>Wei Lai</i>	305
Hybrid Improper Ferroelectricity: A Theoretical, Computational, and Synthetic Perspective <i>Nicole A. Benedek and Michael A. Hayward</i>	331
Using Severe Plastic Deformation to Produce Nanostructured Materials with Superior Properties <i>Ruslan Z. Valiev, Boris Straumal, and Terence G. Langdon</i>	357
Recent Advances in Understanding Diffusion in Multiprincipal Element Systems <i>Anuj Dash, Alope Paul, Sandipan Sen, Sergiy Divinski, Julia Kundin, Ingo Steinbach, Blazej Grabowski, and Xi Zhang</i>	383
Biomaterialized Materials for Sustainable and Durable Construction <i>Danielle N. Beatty, Sarah L. Williams, and Wil V. Sruhar III</i>	411
Brittle Solids: From Physics and Chemistry to Materials Applications <i>Brian R. Lawn and David B. Marshall</i>	441
Small-Scale Mechanical Testing <i>Vikram Jayaram</i>	473
Material Flows and Efficiency <i>Jonathan M. Cullen and Daniel R. Cooper</i>	525
Architectural Glass <i>Sheldon M. Wiederhorn and David R. Clarke</i>	561

Indexes

Cumulative Index of Contributing Authors, Volumes 48–52	593
---	-----

Errata

An online log of corrections to *Annual Review of Materials Research* articles may be found at <http://www.annualreviews.org/errata/matsci>